

# Observation of Power Superbroadening of Spectral Line Profiles on IBM Quantum

Ivo S. Mihov<sup>1</sup> and Nikolay V. Vitanov<sup>1</sup>

<sup>1</sup>*Center for Quantum Technologies, Department of Physics,  
Sofia University, 5 James Bourchier blvd, 1164 Sofia, Bulgaria*

(Dated: June 11, 2025)

Power broadening refers to the widening of the spectral line profile in a two-state quantum transition as the strength of the driving field increases. This phenomenon commonly arises in continuous-wave driving when the radiation field's intensity exceeds the transition's saturation intensity and it has been extensively studied in spectroscopy. For pulsed-field excitation, the spectral response of the quantum system may differ significantly: while a rectangular-shaped pulse leads to a linear power broadening, pulses with smooth shapes show significantly reduced power broadening, for instance, logarithmic for the Gaussian shape and none for the hyperbolic-secant shape. Recently [Phys. Rev. Lett. **132**, 020802 (2024)], in a dramatic paradigm shift, we have demonstrated experimentally that for Lorentzian-shaped pulses, the opposite effect — power narrowing — takes place: the width of the spectral profile decreases when the driving pulse amplitude increases, with a narrowing factor of as much as 10 observed.

While in high-resolution spectroscopy the push is for eliminating or even inverting the power broadening, there are applications where it is used to an advantage for it facilitates off-resonance excitation. Here, we present a number of shaped pulses that exhibit power broadening much greater than that of the rectangular pulse of the same pulse area. They are grouped in two families of pulse shapes. In particular, in regard to the width of the second Rabi oscillation maximum, the quadratic pulse family shows an increase by a factor of 3.3 whereas the even-exponent pulse family exhibits an increase by a factor of more than 3.5.

## I. INTRODUCTION

Power broadening is a crucial phenomenon in quantum control, causing significant interaction between light and matter in a broader frequency spectrum away from resonance. While it is often associated with undesirable effects, such as reduced sensitivity in high-resolution spectroscopy and a cause for unwanted transitions in qubit control, there are applications where it is found to be beneficial. For instance, the same mechanism by which it activates unwanted transitions can be used to enable weak but desired transitions. One such application is laser cooling, where power broadening facilitates effective transitions even with large detunings [1–4]. Additionally, power broadening enables the preparation of certain quantum states in cases where necessary transitions are not accessible otherwise [5]. Finally, power broadening is widely used in spectroscopy to effectively increase the width of narrow resonance peaks that are difficult to detect, enabling their capture and accurate measurement [6–9]. Power-broadened slowing of atoms and molecules plays a key role in robust loading of particles into magneto-optical traps (MOTs) [10–14]. By helping the interaction occur in a broader range of frequencies, the resonance requirement becomes less strict. Therefore, interactions that are otherwise hindered by the resonance condition are enabled.

The power broadening effect has been a research area of interest in quantum physics and spectroscopy ever since early studies on the phenomenon [15–21]. Theoretical interest in the effect has never ceased [22–30]. A substantial body of research has focused on mitigating its effects to increase the precision of various spectroscopic

techniques [31–34]. Indeed, relaxing the resonance condition complicates the accurate determination of the natural frequency, which is fundamental to high-resolution spectroscopy. The impact is generally negative, as it forces spectroscopists to limit the power of the pulses they use for finding the spectral line width, which results in very long data acquisition times, often many weeks and months [35].

Off-resonant qubit excitations are affected by the temporal shape of the Rabi frequency envelope. Hence, the pulse shape properties have long been used to solve common problems in quantum systems, such as leakage, crosstalk, noise sensitivity etc [31, 32, 39–48]. A promising technique for exerting control on the lineshape, pulse shaping allows to reduce or completely eliminate the power broadening of the qubit spectral line. Gaussian, Sine, Sine<sup>2</sup> and other temporal pulse envelopes can be used to diminish it, while the sech pulse halts it completely [24, 32, 36]. Some earlier works even study the potential of pulse shape families that reverse the power broadening [31, 37, 38], introducing the concept of power narrowing using Lorentzian and Lorentzian-based temporally-shaped pulses.

In this work, we investigate how to achieve the opposite effect — generation of maximal power broadening. Starting from the most common example of a linear-broadening-generating rectangular pulse shape, we aim to increase the non-adiabaticity of the pulse envelope, a metric that is shown in Sec. III to predict the degree of power broadening caused by the utilized pulse. We achieve stronger power broadening than the one produced by rectangular pulse shapes with the help of two families of pulse shapes with inherent highly non-

adiabatic artefacts.

## II. ADIABATIC EVOLUTION IN TWO-STATE SYSTEMS

### A. Two-State Schrödinger Equations

In a two-state quantum system, the time-dependent Schrödinger equation governs the evolution of the state vector  $\mathbf{C}(t)\rangle$  given by the equation

$$i\frac{d}{dt}\mathbf{C}(t) = \mathbf{H}(t)\mathbf{C}(t), \quad (1)$$

where  $\mathbf{H}(t)$  is the time-dependent Hamiltonian of the system and  $\mathbf{C}(t) = [c_1(t), c_2(t)]^T$  is the wavevector, consisting of  $c_1(t)$  and  $c_2(t)$  – the (complex) probability amplitudes of the two states.

### B. Hamiltonian in Two-State System

The Hamiltonian for a two-state system in the rotating-wave approximation (RWA) can be represented as

$$\mathbf{H}(t) = \frac{1}{2} \begin{bmatrix} -\Delta(t) & \Omega(t) \\ \Omega^*(t) & \Delta(t) \end{bmatrix}, \quad (2)$$

where  $\Delta(t)$  is the detuning and  $\Omega(t)$  is the Rabi frequency. Its eigenvalues are

$$\varepsilon_{\pm}(t) = \pm \frac{1}{2} \sqrt{\Delta^2(t) + \Omega^2(t)}. \quad (3)$$

In the context of pulse shaping, both  $\Delta$  and  $\Omega$  can vary with time. Substituting this Hamiltonian into Eq. (1), we obtain the two-level Schrödinger system of equations

$$\begin{aligned} 2i\dot{c}_1(t) &= -\Delta(t)c_1(t) + \Omega(t)c_2(t), \\ 2i\dot{c}_2(t) &= \Omega^*(t)c_1(t) + \Delta(t)c_2(t), \end{aligned} \quad (4)$$

where the dot over the probability amplitudes  $c_1(t)$  and  $c_2(t)$  represents the derivative of the corresponding variable with respect to time.

### C. Adiabatic Evolution

Adiabatic evolution occurs when the system's Hamiltonian changes slowly enough over time so the system remains in an instantaneous eigenstate of  $H(t)$ , provided it started in one. This implies that the system avoids transitions between eigenstates, evolving within the same eigenstate [50]. This abstinence from transitioning only occurs in the adiabatic basis, while in the bare basis, transitions between the ground and excited states may occur only in the presence of chirp, change in detuning,  $\dot{\Delta}(t)$ .

### D. Boosting power broadening – non-adiabaticity

The adiabatic condition requires the change in the Hamiltonian to be slow relative to the energy difference between the eigenstates. If this is satisfied, the system evolves adiabatically. In quantum power broadening and superbroadening, pulse shaping affects both the Rabi frequency  $\Omega(t)$  and the adiabaticity conditions, making it possible to maintain control over transitions and achieve substantial broadening effects. This connection has been studied in relation to power narrowing in Ref. [31]. Expanding on the ideas in that study, we regard power broadening a consequence of the nonadiabatic nature of the pulse shape. Therefore, we demand significant non-adiabaticity to achieve strong power broadening. This is the reason we look for pulse shapes that have more non-adiabatic artifacts than the rectangular pulse and naturally violate the adiabatic condition

$$\underbrace{\sqrt{\Omega^2(t) + \Delta^2(t)}}_{\varepsilon_1(t)} \gg \underbrace{\frac{\dot{\Omega}(t)\Delta(t) + \Omega(t)\dot{\Delta}(t)}{\Omega^2(t) + \Delta^2(t)}}_{\vartheta_1(t)}. \quad (5)$$

Developing on this notion, we notice that the larger  $\dot{\Omega}(t)$  is, the less adiabatic the system is. Thus, we seek pulse shapes that exhibit sudden Rabi frequency changes concurrent with small Rabi frequencies.

The theory of adiabaticity begins with the construction of the adiabatic states — the (time-dependent) eigenstates of the Hamiltonian [44]. The original diabatic basis is related to the adiabatic one by the transformation matrix  $\mathbf{R}(\vartheta_1)$ :

$$\mathbf{C}(t) = \mathbf{R}(\vartheta_1(t))\mathbf{A}_1(t), \quad (6)$$

where

$$\mathbf{R}(\vartheta_1) = \begin{bmatrix} \cos \vartheta_1 & \sin \vartheta_1 \\ -\sin \vartheta_1 & \cos \vartheta_1 \end{bmatrix}, \quad (7)$$

with

$$\vartheta_1(t) = \frac{1}{2} \arctan \left( \frac{\Omega(t)}{\Delta} \right) \quad (0 \leq \vartheta_1(t) \leq \pi/4). \quad (8)$$

Substituting the diabatic states  $\mathbf{C}(t)$  into the Schrödinger equation (1), we rearrange and obtain an analogical equation, extracting the adiabatic Hamiltonian

$$\mathbf{H}_1(t) = \mathbf{R}(-\vartheta_1)\mathbf{H}\mathbf{R}(\vartheta_1) - i\hbar\mathbf{R}(-\vartheta_1)\frac{d}{dt}\mathbf{R}(\vartheta_1) \quad (9)$$

$$= \begin{pmatrix} \varepsilon_-(t) & -i\dot{\vartheta}_1(t) \\ i\dot{\vartheta}_1(t) & \varepsilon_+(t) \end{pmatrix}, \quad (10)$$

where  $\varepsilon_{\pm}$  are the eigenvalues of the diabatic Hamiltonian from Eq. (3). Now we have a Hamiltonian which becomes diagonal (i.e. we stay in the adiabatic states) if  $\varepsilon_+ - \varepsilon_- \gg |\dot{\vartheta}_1|$ . Since  $\varepsilon_+(t) - \varepsilon_-(t) = \varepsilon_1(t) = \sqrt{\Omega^2(t) + \Delta^2}$ , we obtain the adiabatic condition, shown in Eq. (5).

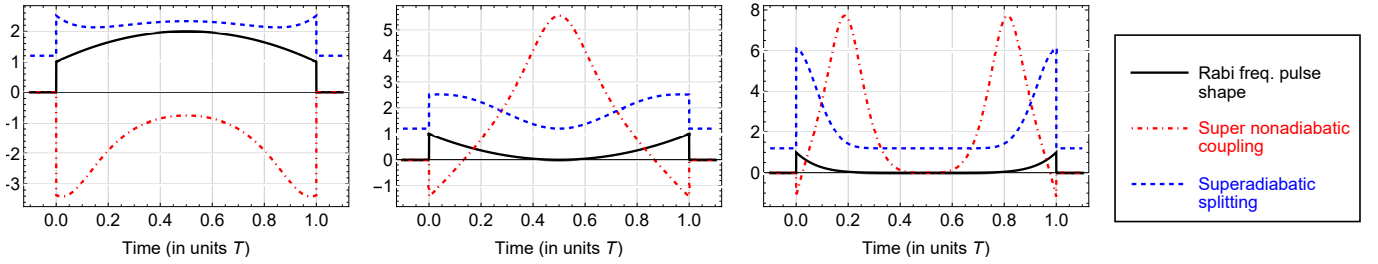


FIG. 1: [Color online] The super-nonadiabatic coupling and superadiabatic splitting are shown for three different pulse shapes: (from left to right) a quadratic with  $\beta = -1$ , a quadratic with  $\beta = 1$  and an even-power pulse with  $N = 3$ .

### E. Superadiabatic basis

The superadiabatic bases [44] can be used to compare the superadiabaticity of the current pulse shapes. The superadiabatic bases are obtained by repeated diagonalization of the previous-order superadiabatic bases. We regard the adiabatic basis an order-1 superadiabatic basis, and use it as a starting point in order to retrieve the  $n = 2$  basis. We begin with a phase transformation on the Hamiltonian,

$$\mathbf{F} = \begin{bmatrix} e^{-i\pi/4} & 0 \\ 0 & e^{i\pi/4} \end{bmatrix}, \quad (11)$$

Thus, we get the transformation  $\mathbf{H}_1(t) \rightarrow \mathbf{H}_2(t) = \mathbf{F}^\dagger \mathbf{H}_1(t) \mathbf{F}$ , as well as some analogues of the  $n = 1$  variables,

$$\begin{aligned} \Delta &\rightarrow \varepsilon_1(t), \\ \Omega(t) &\rightarrow 2\dot{\vartheta}_1(t), \\ \mathbf{C}(t) &\rightarrow \mathbf{A}_1(t). \end{aligned} \quad (12)$$

Indeed, all of the adiabatic variables have their analogues,

$$\begin{aligned} \vartheta_1(t) &\rightarrow \vartheta_2(t), \\ \varepsilon_1(t) &\rightarrow \varepsilon_2(t), \\ \mathbf{A}_1(t) &\rightarrow \mathbf{A}_2(t), \\ \mathbf{H}_1(t) &\rightarrow \mathbf{H}_2(t), \\ \eta_1 &\rightarrow \eta_2. \end{aligned} \quad (13)$$

The superadiabatic condition becomes

$$\underbrace{\sqrt{4\dot{\vartheta}_1^2(t) + \varepsilon_1^2(t)}}_{\varepsilon_2(t)} \gg \underbrace{\frac{2\ddot{\vartheta}_1(t)\varepsilon_1(t) + 2\dot{\vartheta}_1(t)\dot{\varepsilon}_1(t)}{4\dot{\vartheta}_1^2(t) + \varepsilon_1^2(t)}}_{\dot{\vartheta}_2(t)}. \quad (14)$$

By repeating the process, we can also obtain the higher-order superadiabatic bases [44].

### III. THE QUADRATIC AND THE EVEN EXPONENT PULSE SHAPES

Based on the sought properties in the superadiabatic basis, two families of temporal pulse shapes are introduced—the quadratic and the even exponent pulse shapes. The quadratic pulse shape resembles a rectangular pulse with an added parabolic term, as illustrated in Fig. 2a. Despite the simplicity of its crude form –  $\Omega(t) \propto 1 + \beta t^2$ , where  $\beta$  is a parameter – the normalized expression for this pulse shape is

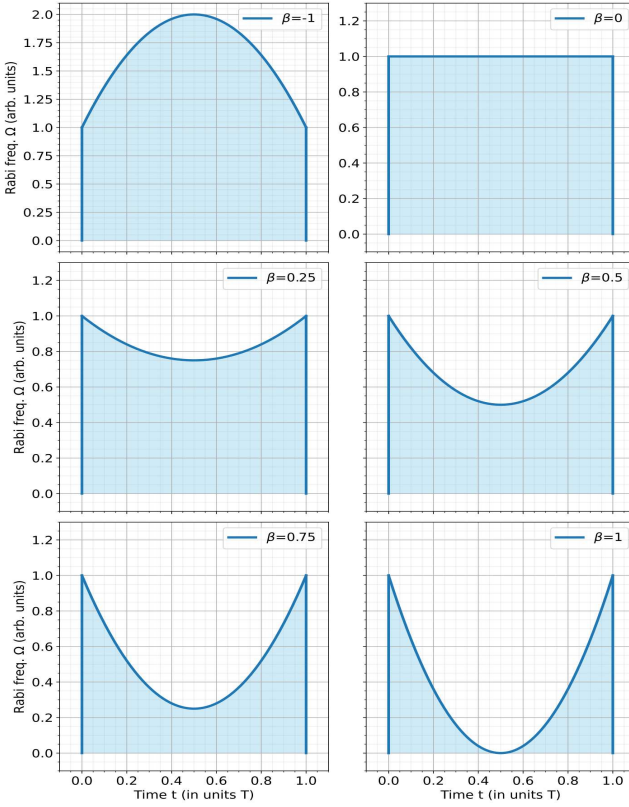
$$\Omega(t) = \Omega_0 \left\{ 1 + \beta \left[ \left( \frac{t - T/2}{T/2} \right)^2 - 1 \right] \right\}, \quad (15)$$

where  $\beta$  controls the degree of concavity or convexity of the added parabola, and  $T$  is the pulse duration. The parameter  $\beta$  has an applicability range  $\beta \in (-\infty, 1]$ . The upper boundary  $\beta = 1$  represents the case where the midpoint of the pulse touches the  $\Omega(t) = 0$  line. For higher values of  $\beta$ , its Rabi frequency would become negative at the midpoint, an undesirable characteristic, which motivated us to introduce the upper limit of  $\beta$ .

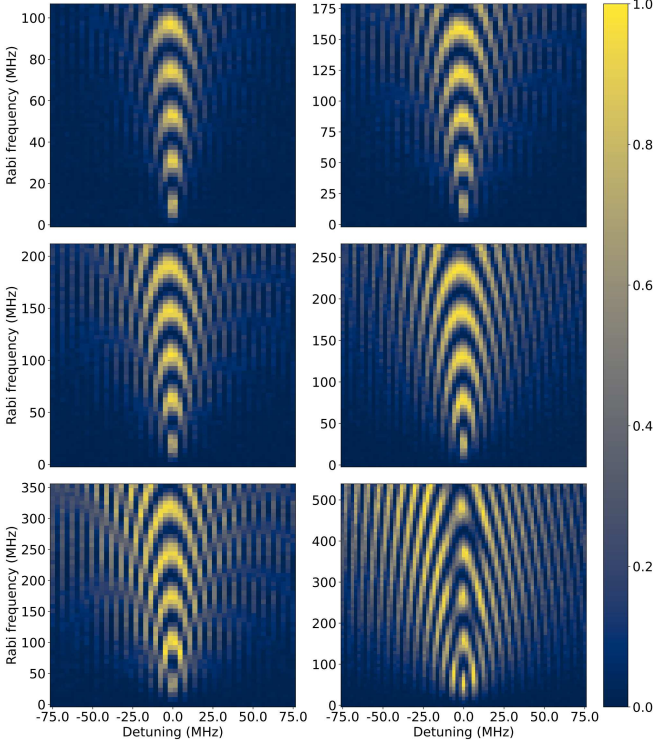
Similarly designed to break the superadiabatic inequality, the even-exponent pulse shape incorporates nonadiabatic features, namely discontinuous jumps at the edges and an inherent zero value at the midpoint of the pulse. Its crude form is  $\Omega(t) \propto t^{2P}$ , but adjusted for unity it becomes

$$\Omega(t) = \Omega_0 \left( \frac{t - T/2}{T/2} \right)^{2P}, \quad (16)$$

where  $P \in \mathbb{N}$  is a parameter, half the exponent of time  $t$ , and controls the width of the pit. With  $P = 0$ , the even exponent (EE) pulse shape becomes the standard rectangular pulse shape, or put alternatively – the pit has zero width. For  $P \gg 1$  the shape approximates two Dirac delta functions time  $T$  apart. For a high exponent  $P$  and the right pulse area, where each of the two horns has area  $\mathcal{A} = \pi/2$ , combining for a total area of  $\pi$ , the pulse can be used to produce Ramsey fringes in the frequency spectrum. Similar to the  $\beta = 1$  case of the quadratic pulse shape, the even-exponent pulse also

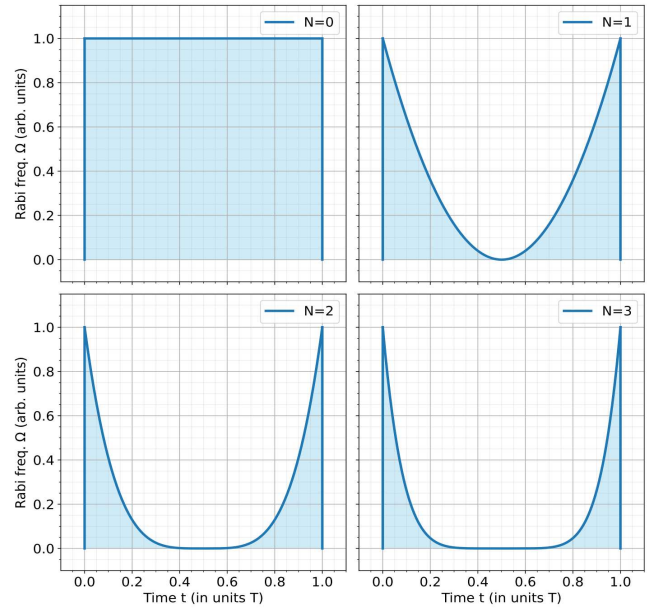


(a) Illustration of the face-changing quadratic pulse shapes with 6 different values of  $\beta$ : -1, 0, 0.25, 0.5, 0.75 and 1.

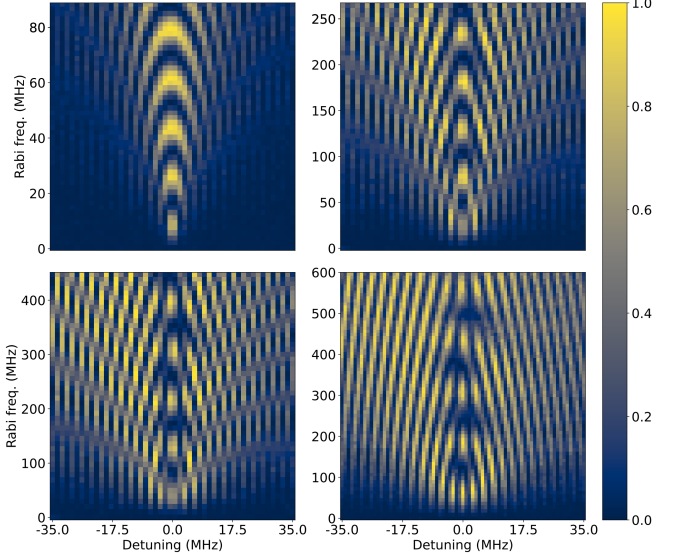


(b) Illustration of the observed excitation landscapes (transition probability against Rabi frequency amplitude and detuning) of face-changing quadratic pulse shapes with 6 different values of  $\beta$ : -1, 0, 0.25, 0.5, 0.75 and 1.

FIG. 2: [Color online] Illustration of the excitation landscapes (bottom) with a legend of the used quadratic pulse shape (top).



(a) Illustration of the even exponent pulse shapes with 6 different values of  $P$ : 0, 1, 2, and 3.



(b) Illustration of the observed excitation landscapes (transition probability against Rabi freq. amplitude and detuning) of even exponent pulse shapes with 4 different values of  $P$ : 0, 1, 2, and 3.

FIG. 3: [Color online] Illustration of the excitation landscapes (bottom) with a legend of the used even exponent pulse shape (top).

inherently reaches zero in the midpoint for all values of its parameter  $P$ .

Interestingly, the  $\beta = -1$  and  $\beta = +1$  quadratic pulse shapes have the same derivatives in magnitude, only the signs are inverted. Intuitively, this could incline us to believe that their representations in the adiabatic basis would not differ and that the adiabatic inequality would

lead to similar conclusions for both of them. However, one can see in Fig. 1 that the superadiabatic inequality is violated by the  $\beta = 1$  quadratic pulse, and by the  $N = 3$  even-power pulse shape but not by the  $\beta = -1$  quadratic pulse shape. This finally allows us to see why the  $\beta = -1$  and  $\beta = +1$  shapes behave differently at  $\Delta \neq 0$ .

### A. Orientation-changing quadratic

The orientation-changing quadratic pulse shapes with  $\beta = -1, 0, 0.25, 0.5, 0.75$  and  $1$  were tested on the 127-qubit IBM quantum computer – *ibm\_sherbrooke*. The detailed list of parameters recorded during the experiment is shown in Sec. A. The duration of all orientation-changing quadratic pulses was  $800 dt$  units—the system time units used in IBM’s Qiskit framework—which corresponds to  $177.8$  ns. As stated previously, the  $\beta = 0$  case of the face-changing quadratic is in fact the constant pulse. It arises from simply turning the pulse generator on and off after time  $T$  and is known for reproducing the common linear power broadening. In line with this hypothesis, we indeed see the common broadening pattern in the top right excitation map of Fig. 2b, corresponding to the  $\beta = 0$  case. It is also evident that as  $\beta$  changes from  $-1$  to  $0$ , the power broadening pattern grows stronger. In the  $\beta = -1$  plot the second maximum is about  $20$  MHz wide, whereas in the  $\beta = 0$  case, a fringe appears at around  $\Delta = \pm 15$  MHz, resulting in a linewidth of  $30$  MHz. The broadening pattern is much stronger in the linewidth of the  $\beta = 1$  pulse, spanning a frequency interval of about  $100$  MHz, or an increase by a factor of about  $3.3$  compared to the rectangular pulse ( $\beta = 0$ ). It is not intuitive that the  $\beta = -1$  case, albeit having the same derivative in magnitude, shows strikingly weaker power broadening than the  $\beta = 1$  case. These two examples form the limiting cases in the experiment, with the  $\beta = 1$  plot having at least  $5$  visible fringes around the second maximum. Both pulse shapes have exactly the same derivatives in magnitude, but their signs are different. In the  $\beta = -1$  case, the derivative is first positive, then negative for the second half of the pulse, while in the  $\beta = 1$  case, they are in the opposite order. This difference may seem insignificant at first, but completely changes the pulse’s appearance in the adiabatic and superadiabatic pictures.

The reason is that the super-nonadiabatic effects in the latter case are stronger around the midpoint of the pulse. This is shown using the superadiabatic basis and its super-nonadiabatic coupling and super-splitting as evident from the comparison in Fig. 1. In the latter case  $\Omega(t)$  is negligible in the midpoint area, while the derivatives  $\dot{\Omega}(t)$  are the same. In the middle plot of Fig. 1, it is clear that the nonadiabatic coupling is higher for the  $\beta = 1$  pulse, which enables the transition even far from resonance.

### B. Even-exponent pulse

The excitation landscapes in Fig. 3b demonstrate progressively stronger power broadening, accompanied by increasingly pronounced fringe patterns. Aiming at higher non-adiabaticity, we evaluated even-exponent pulse shapes with  $P \in \{0, 1, 2, 3\}$  on the 127-qubit IBM quantum computer – *ibm\_sherbrooke*. The values of key parameters recorded throughout the demonstration are listed in Sec. A. The duration of all even-exponent pulses was  $1600 dt$  units or  $355.6$  ns. Notably, for all  $P > 0$ , the Rabi frequency at the pulse midpoint is zero, a distinctive feature of the even-exponent pulse shape. This characteristic enhances the pulse’s nonadiabatic behavior, effectively mimicking a configuration resembling two well-separated pulses, each with an area of  $\pi/2$ , similar to those employed in Ramsey interferometry to generate Ramsey fringes. Taking a look at the width of the spectral lines for a  $\pi$ -area pulse for  $P = 0$  and  $P = 3$ , we see a huge broadening in the  $P = 3$  case. A glance at the first maxima standing at  $\mathcal{A} = \pi$  signals that it broadens from roughly  $8$  MHz wide in the  $P = 0$  case to about  $30$  MHz in the  $P = 3$  case. While the linewidth of the  $3\pi$  pulse is about  $20$  MHz in the  $P = 0$  case, it is wider than the  $70$  MHz scope of the plot depicting the  $P = 3$  case, obtained by taking all visible fringes into account.

Examining the two plots on the bottom row — corresponding to  $P = 2$  (left) and  $3$  (right) — we find that dark nearly vertical lines have started to appear  $\approx 3$  MHz apart due to interference between the left and right horns of the even-exponent pulse. These lines are to increase both in number and contrast with higher numbers of  $P$ .

## IV. CONCLUSIONS

In conclusion, we have presented viable and simple pulse shaping alternatives to the commonly used rectangular pulse shape. Without significant shifts in duration and shape, we employ two new families of temporal pulse shapes to observe threefold broadening in the effective linewidth of the qubit, measured at the same, minimal pulse area of  $\pi$ . These pulse shapes are at the heart of the newly demonstrated power superbroadening phenomenon, a stronger variation of power broadening. It can be used in cases where power broadening is beneficial, contributing to its positive effects.

Usually, these are cases where power broadening is used to excite off-resonant transitions or look for resonant frequencies in a broad interval. Some interesting applications also include laser cooling, where off-resonant transitions supply less energy than the transition needs, thereby extracting energy from the system and decreasing its temperature. The method described here builds upon the commonly employed power broadening effect to boost it further and promise to enhance its function in many applications.

## V. ACKNOWLEDGMENTS

We gratefully acknowledge the Karoll Knowledge Foundation for providing financial support to I.S.M. during the preparation of this manuscript. Their contribution was invaluable, not only to this work but in encouraging the author's ongoing scientific endeavors. This research is supported by the Bulgarian national plan for recovery and resilience, Contract No. BG-RRP-2.004-

0008-C01 (SUMMIT), Project No. 3.1.4, and by the European Union's Horizon Europe research and innovation program under Grant Agreement No. 101046968 (BRISQ). We acknowledge the use of IBM Quantum services and the supercomputing cluster PhysOn at Sofia University for this work.

The views expressed are those of the authors, and do not reflect the official policy or position of IBM or the IBM Quantum team.

---

[1] F. Lindenfelser, M. Marinelli, V. Negnevitsky, S. Ragg and J. P. Home, *New J. Phys.* **19**, 063041 (2017).

[2] O. N. Prudnikov, R. Ya. Il'enkov, A. V. Taichenachev, and V. I. Yudin, *Phys. Rev. A* **99**, 023427 (2019).

[3] S. A. Fedorov, G. A. Vishnyakova, E. S. Kalganova, D. D. Sukachev, A. A. Golovizin, D. O. Tregubov, K. Yu. Khabarova, A. V. Akimov, N. N. Kolachevsky, and V. N. Sorokin, *Appl. Phys. B* **121**, 275 (2015).

[4] Y. Mao, J. Xu, S. Guan, H. Ji, W. Liu, D. Chen, Q. Gong, Y. Quan, X. Long, H. Luo, Z. Tan, arXiv:2312.09635 (2023).

[5] H. Park, E. S. Shuman, and T. F. Gallagher, *Phys. Rev. A* **84**, 052708 (2011).

[6] J. J. Berry, M. J. Stevens, R. P. Mirin, and K. L. Silverman, *Appl. Phys. Lett.* **88**, 061114 (2006).

[7] S. Ya. Tochitsky, C. Filip, R. Narang, C. E. Clayton, K. A. Marsh, and C. Joshi, *Opt. Lett.* **26**, 813 (2001).

[8] J. Levine, M. R. Savina, T. Stephan, N. Dauphas, A. M. Davis, K. B. Knight, and M. J. Pellin, *Int. J. Mass. Spectr.* **288**, 36 (2009).

[9] O. G. Calderón, S. Melle, M. A. Antón, F. Carreño, F. Arrieta-Yáñez, and E. Cabrera-Granado, *Phys. Rev. A* **78**, 053812 (2008).

[10] M. Zhu, C. W. Oates, and J. L. Hall, *Phys. Rev. Lett.* **67**, 46 (1991).

[11] M. Yeo, M. T. Hummon, A. L. Collopy, B. Yan, B. Hemmerling, E. Chae, J. M. Doyle, and J. Ye, *Phys. Rev. Lett.* **114**, 223003 (2015).

[12] T. Ravi, R. C. Das, H. V. Bhusane, S. Roy, K. Pandey, arXiv:2505.14301 (2025).

[13] H. J. Williams, S. Truppe, M. Hambach, L. Caldwell, N. J. Fitch, E. A. Hinds, B. E. Sauer, and M. R. Tarbutt, *New J. Phys.* **19**, 113035 (2017).

[14] S. Truppe, H. J. Williams, N. J. Fitch, M. Hambach, T. E. Wall, E. A. Hinds, B. E. Sauer, and M. R. Tarbutt, *New J. Phys.* **19**, 022001 (2017).

[15] R. G. Breene, *The shift and shape of spectral lines* (Pergamon, New York, 1961).

[16] R. G. Breene, *Theories of spectral line shapes* (Wiley, New York, 1981).

[17] R. G. Breene, H. R. Zaidi, *Physics Today* **34**, 99 (1981).

[18] L. Allen, J. H. Eberly, *Optical resonance and two-level atoms* (Dover, New York, 1975).

[19] B. W. Shore, *The Theory of Coherent Atomic Excitation* (Wiley, New York, 1990).

[20] M. L. Citron, H. R. Gray, C. W. Gabel, and C. R. Stroud, Jr., *Phys. Rev. A* **16**, 1507 (1977).

[21] J. C. Bergquist, *Doppler-free spectroscopy* (Chapter 13) (Academic Press, Boulder, 1996). Available online: <https://tf.nist.gov/general/pdf/1125.pdf>.

[22] C. J. Foot, *Atomic Physics* (Oxford University Press, 2005)

[23] P. W. Milonni and J. H. Eberly, *Laser Physics* (Wiley, 2010).

[24] N. V. Vitanov, B. W. Shore, L. P. Yatsenko, K. Böhmer, T. Halfmann, T. Rickes, and K. Bergmann, *Opt. Commun.* **199**, 117 (2001).

[25] T. Halfmann, T. Rickes, N. V. Vitanov, and K. Bergmann *Opt. Commun.* **220**, 353 (2003).

[26] A. Harth, *IEEE J. Quant. Electr.* **31**, 894 (1995).

[27] C. Roy and S. Hughes, *Phys. Rev. X* **1**, 021009 (2011).

[28] J. Levine, *Spectrochim. Acta B: At. Spectr.* **69**, 61 (2012)

[29] R. J. Bettles, M. D. Lee, S. A. Gardiner, and J. Ruostekoski, *Commun. Phys.* **3**, 141 (2020).

[30] C. W. S. Conover, *Phys. Rev. A* **84**, 063416 (2011).

[31] I. S. Mihov and N. V. Vitanov, *Phys. Rev. Lett.* **132**, 020802 (2024).

[32] I. S. Mihov and N. V. Vitanov, *Phys. Rev. A* **108**, 042604 (2023).

[33] H. M. Florez, L. S. Cruz, M. H. G. de Miranda, R. A. de Oliveira, J. W. R. Tabosa, M. Martinelli, and D. Felinto, *Phys. Rev. A* **88**, 033812 (2013).

[34] M. E. Reimer, G. Bulgarini, A. Fognini, R. W. Heeres, B. J. Witek, M. A. M. Versteegh, A. Rubino, T. Braun, M. Kamp et al., *Phys. Rev. B* **93**, 195316 (2016).

[35] L. S. Dreissen, C.-H. Yeh, H. A. Fürst, K. C. Grenseemann, and T. E. Mehlstäubler, *Nat. Commun.* **13**, 7314 (2022).

[36] N. Rosen and C. Zener, *Phys. Rev.* **40**, 502 (1932).

[37] E. J. Robinson, *J. Phys. B: Atom. Mol. Phys.* **18**, 3687 (1985).

[38] I. I. Boradjiev and N. V. Vitanov, *Opt. Commun.* **288**, 91 (2013).

[39] J. Zhu, X. Laforgue, X. Chen and S. Guérin, *J. Phys. B: At. Mol. Opt. Phys.* **55**, 194001 (2022).

[40] M. Harutyunyan, F. Holweck, D. Sugny, and S. Guérin, *Phys. Rev. Lett.* **131**, 200801 (2023).

[41] F. Peyraut, F. Holweck, and S. Guérin, *Entropy* **25**, 212 (2023).

[42] M. Kuzmanović, I. Björkman, J. J. McCord, S. Dogra, and G. S. Paraoanu, *Phys. Rev. Research* **6**, 013188 (2024).

[43] J. J. McCord, M. Kuzmanović, G. S. Paraoanu, arXiv:2504.16646 (2025).

[44] I. I. Boradjiev and N. V. Vitanov, *Phys. Rev. A* **88**, 013402 (2013).

[45] A. Saharyan, B. Rousseaux, Z. Kis, S. Stryzhenko, and S. Guérin, *Phys. Rev. Research* **5**, 033056 (2023).

Day	$T_1$ (μs)	$T_2$ (μs)	Readout Error (%)
27 Nov	393.66	596.88	0.66
29 Nov	321.33	697.45	0.76
1 Dec	316.42	492.27	0.58
3 Dec	256.01	287.59	2.05
5 Dec	347.80	468.87	1.58

TABLE I: Hardware parameter values for qubit 46 of the *ibm\_sherbrooke* quantum system on 5 service days in 2024.

- [46] I. S. Mihov and N. V. Vitanov, Phys. Rev. A **110**, 052609 (2024)
- [47] F. Motzoi, J. M. Gambetta, P. Rebentrost, and F. K. Wilhelm, Phys. Rev. Lett. **103**, 110501 (2009).
- [48] B. Li, T. Calarco, and F. Motzoi, npj Quantum Information **10**, 66 (2024).
- [49] N. V. Vitanov, B. W. Shore, and L. P. Yatsenko, Ukr. J. Phys. **54**, 53 (2009).
- [50] M. Born and V. A. Fock, Z. Phys. A **51**, 165 (1928).
- [51] IBM Quantum (2022), URL <https://quantum-computing.ibm.com>.
- [52] J. Koch, T. M. Yu, J. Gambetta, A. A. Houck, D. I. Schuster, J. Majer, A. Blais, M. H. Devoret, S. M. Girvin and R. J. Schoelkopf, Phys. Rev. A **76**, 042319 (2007).

### Appendix A: Quantum processor specs

The two pulse shape families were tested against measurements on qubit 46 of the 127-qubit transmon quantum processor – IBM’s *ibm\_sherbrooke*, an Eagle r3 Processor [51, 52].

Due to the limited free slots on the hardware, the measurements were taken on 5 different days. The  $P = 0$  even-exponent pulse was taken on 27 Nov 2024, while the  $P = 1, 2, 3$  pulses were recorded on 29 Nov 2024.

The  $\beta = -1$  and 0 quadratic pulses were demonstrated on 1 Dec 2024, the  $\beta = 1$  pulse test was performed on 3 Dec 2024, and the  $\beta = 0.75, 0.5$  and 0.25 quadratic pulses — on 5 Dec 2024.

Qubit 46 of the *ibm\_sherbrooke* system had a excitation frequency of 4.6741 GHz and an anharmonicity of -0.3134 GHz, both of which were constant over the days of the demonstration. The  $T_1$  decoherence times were between 250 and 400 μs, while the  $T_2$  were even better — between 280 and 700 μs. A more detailed breakdown of the parameters on each day of the demonstration can be found in Table I. The recorded values imply a  $T_2$ -limited linewidth of several kHz, which is tiny compared to a linewidth between 5 and 150 MHz. Thus, the dephasing effects in this demonstration are insignificant.

We use the Qiskit Pulse framework for Python to access the low-level settings of the quantum processor, reproducing the target pulse shapes. Albeit freely available, the framework has some limitations due to its characteristics:

- (i) a soft upper limit on the total duration of the pulse (usually at several μs);
- (ii) an upper limit on the amplitude (limited to 1 in Qiskit’s arbitrary units);
- (iii) a lower limit on the pulse duration caused by the discretization – 2/9 ns;
- (iv) basis measurements of the first two levels only, i.e. all the leakage is summed together with the excited level population.

The framework accommodates a wide choice of resources that can be used to construct gates, methods, and algorithms. Using some neat workarounds, the aforementioned limitations may not pose a problem, rather an immediate impediment.